

## Infrared and Raman spectra of the IV-VI compounds SnS and SnSe

H. R. Chandrasekhar, R. G. Humphreys, U. Zwick, and M. Cardona

Max-Planck-Institut für Festkörperforschung, Stuttgart 80 Federal Republic of Germany

(Received 7 October 1976)

The results of Raman scattering and infrared reflectivity measurements on the IV-VI layer-type semiconductors SnS and SnSe are presented. The infrared-active TO, the associated LO-phonon frequencies, and the dielectric constants for all three principal polarizations have been determined from a Kramers-Kronig analysis of the reflectivity data. The symmetries of the zone-center phonons observed in the different polarization configurations are in agreement with the group-theoretical analysis of the  $D_{2h}^{16}$  space group of these compounds. Despite the center of inversion symmetry in this structure, some infrared- and Raman-active modes are found to be nearly degenerate, suggesting the importance of the layerlike character in these compounds as in the isomorphous GeS and GeSe. A comparison of the phonon frequencies of the corresponding modes in the spectra of SnS and SnSe, or GeS and GeSe, indicates that the frequencies vary as a power ( $-2.2$ ) of the lattice constant.

### I. INTRODUCTION

Among the IV-VI compounds, germanium sulphide (GeS), germanium selenide (GeSe), tin sulphide (SnS), and tin selenide (SnSe) have the orthorhombic structure with eight atoms per unit cell<sup>1-3</sup> forming double-layer planes normal to the longest axis. Raman scattering,<sup>4,5</sup> reflectivity spectra in the infrared<sup>4</sup> and in the range 0.1–30 eV,<sup>6</sup> band-edge absorption spectra,<sup>7</sup> and the electron-energy-loss spectra<sup>8</sup> of single-crystal GeS have been reported. Electrical-resistivity and Hall-coefficient measurements,<sup>9</sup> unpolarized<sup>10</sup> and polarized infrared reflectivity spectra,<sup>11,12</sup> Raman scattering,<sup>11</sup> and the band-edge absorption spectra<sup>13</sup> of GeSe have been published. The optical-absorption edge,<sup>14-16</sup> unpolarized infrared transmission<sup>17</sup> and reflectivity<sup>17,18</sup> spectra of SnS, and the electrical resistivity and Hall coefficient<sup>19</sup> and optical-absorption edge<sup>14,20</sup> of SnSe have been investigated. A study of the optical transmission from 1 to 6 eV, electron-energy-loss spectra from 1 to 23 eV,<sup>21</sup> and the lattice-dynamical calculations<sup>22</sup> for GeS, GeSe, SnS, and SnSe have also been undertaken.

The unit-cell dimensions, and the fundamental energy gaps at room temperature of GeS, GeSe, SnS, and SnSe are shown in Table I. The crystal structure can be viewed as a severely distorted rocksalt structure with each atom having three strongly bonded neighbors within its own layer and three more distant neighbors, one of which lies in an adjacent layer. The three-dimensional space group of these compounds is  $D_{2h}^{16}$  with the center of inversion lying between the double layers. If the interlayer forces are ignored the point group of the two-dimensional space group<sup>23</sup> is  $C_{2v}$  and has no inversion center. The two symmetries lead to different selection rules for the phonon

spectra. The degeneracies due to layer symmetry are lifted when coupling between layers is introduced (Davydov splitting) as the modes split into infrared-active and Raman-active doublets. This splitting provides a means of probing the relative strengths of the interlayer and intralayer forces.

In this paper we present, for the first time, the Raman scattering and infrared reflectivity spectra, the zone-center optical-phonon frequencies and dielectric constants of SnS and SnSe for all principal polarizations. The Davydov splittings of the corresponding infrared and Raman-active phonon frequencies are determined. Ratios of various pairs of interlayer and intralayer force constants are estimated. These results are compared with the corresponding ones for GeS and GeSe, in the context of the two-dimensionality or "layer-type" behavior of these compounds.

### II. EXPERIMENT

Polarized Raman and infrared reflectivity spectra were measured on oriented single crystals at room temperature. The SnS samples could be cleaved easily. The measurements on the cleavage plane ( $c$  plane) were made with freshly cleaved

TABLE I. Lattice parameters (in Å) and the energy gap (in eV) at room temperature of GeS, SnS, GeSe, and SnSe (see Ref. 1).

	GeS	SnS	GeSe	SnSe
$a$	4.29	4.33	4.38	4.46
$b$	3.64	3.98	3.82	4.19
$c$	10.42	11.18	10.79	11.57
$E_g$	1.65 <sup>a</sup>	1.08 <sup>b</sup>	1.53	0.90 <sup>c</sup>

<sup>a</sup>Reference 6.

<sup>b</sup>Reference 15.

<sup>c</sup>Reference 14.

surfaces. The measurements on  $a$  and  $b$  planes of SnS and SnSe and also the  $c$  plane of SnSe were carried out on mechanically polished and etched surfaces.

Raman spectra were recorded using a back scattering geometry. A Spex Triple monochromator or a Jarrel-Ash double monochromator equipped with holographic gratings, and a cooled ITT FW-130 photomultiplier, with associated photon-counting electronics, were used. Various frequencies in the red and near infrared of a Kr<sup>+</sup> laser (Spectra Physics Model 171 or 165) were used as the excitation source. Owing to the narrow band gap (see Table I), and the resulting high absorption coefficient, it was necessary to employ signal-averaging procedures and repeat the spectra with different laser frequencies to check the reproducibility of some weak lines.

The infrared reflectivity spectra were measured on a Polytec FIR 30 Fourier spectrometer in the frequency range of 20–450 cm<sup>-1</sup> and a Perkin-Elmer (Model 180) grating spectrophotometer in the range of 200–4000 cm<sup>-1</sup>. The spectra for  $\vec{E}$ , the electric vector, parallel to the  $a$  or  $b$  axis were taken on an oriented cleavage plane using a wire-grid polarizer. The spectrum for  $\vec{E} \parallel \vec{c}$  was taken on a polished  $a$  or  $b$  face. The back surface of the sample was wedged or rounded in order to prevent interference fringes and spurious contributions to the reflectivity.

### III. EXPERIMENTAL RESULTS

A factor-group analysis of the three-dimensional space group  $D_{2h}^{16}$  reveals that of the 21 optical pho-

nons, 2 are inactive, 7 are infrared active, and 12 are Raman active. The symmetries, multiplicities, and the selection rules for the observation of these phonons are shown in Table II. Also shown in this table are the compatibility relations which exist between phonons for the point groups  $C_{2v}$  and  $D_{2h}$ .<sup>24</sup>

Figures 1 and 2 show the Raman spectra of SnS and SnSe, respectively, for various scattering geometries. The incident laser beam was always parallel to one of the principal axes  $\vec{a}$ ,  $\vec{b}$ , or  $\vec{c}$ . In the notation  $x(yz)\bar{x}$ , for example,  $x$  and  $\bar{x}$  denote the direction of the incident and scattered direction of radiation, respectively;  $y$  and  $z$  indicate the electric polarization vector of the incident and scattered photons. The number of observed phonons of  $A_g$ ,  $B_{3g}$ , and  $B_{1g}$  modes is consistent with group-theoretical predictions. Four phonons are predicted to be observed in the  $B_{2g}$  configuration; three Raman peaks were clearly observed at 70, 85, and 290 cm<sup>-1</sup> for SnS. The intensity of these modes was an order of magnitude smaller than that of the  $A_g$  modes. However, their presence was confirmed by repeated measurements with different laser frequencies. The spectra for SnSe did not show any clearly discernible  $B_{2g}$  modes. Various attempts to observe the spectra with different exciting laser frequencies and long signal-averaging procedures were unsuccessful. We attribute this to the weak Raman tensor in this configuration. That this was not due to poor surface quality was clear from the strength of the  $A_g$  modes observed from the same surface. It should be noted that the  $B_{2g}$  modes were very weak<sup>4,11</sup> in

TABLE II. Compatibility relation between the corresponding phonon modes of the layer-symmetry group DG32 (point group  $C_{2v}$ ) and the space group  $D_{2h}^{16}$  (point group  $D_{2h}$ ). The infrared and Raman selection rules are also shown. The notation for Raman selection rules indicates the polarization of the incident and scattered photons for a back scattering configuration.

Layer symmetry	Crystal symmetry	Selection rules	
		Infrared	Raman
$3A_1$	$3A_g$	...	$(aa), (bb), (cc)$
	$3B_{1u}$	$\vec{E} \parallel \vec{a}$	...
$2A_2$	$2B_{1g}$	...	$(bc)$
	$2A_u$	Inactive	...
$3B_1$	$3B_{2g}$	...	$(ac)$
	$3B_{3u}$	$\vec{E} \parallel \vec{c}$	...
$1B_2$	$1B_{3g}$	...	$(ab)$
	$1B_{2u}$	$\vec{E} \parallel \vec{b}$	...
$1A_1, 1B_1, 1B_2$ (Translation)	$1B_{3g}$	...	$(ab)$
	$1B_{2g}$	...	$(ac)$
	$1A_g$	...	$(aa), (bb), (cc)$
	$1B_{1u}, 1B_{2u}, 1B_{3u}$	Translation	...

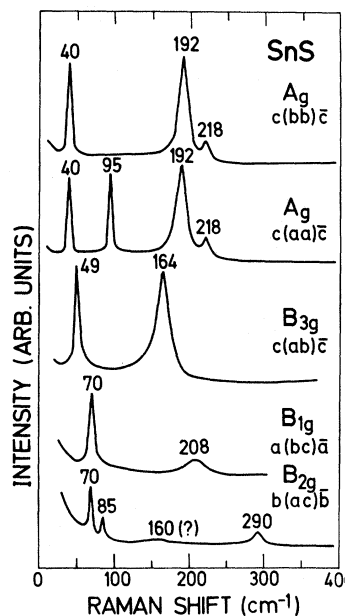


FIG. 1. Room-temperature Raman spectra of SnS. The notation  $x(yz)\bar{x}$  indicates the incident direction of exciting radiation, the polarization of the incident and scattered radiation, and the direction of the scattered radiation, respectively. The intensity scales of the spectra for different modes are not the same. The exciting radiation used was  $6471 \text{ \AA}$ .

the case of GeS and GeSe also.

Figures 3 and 4 show the infrared reflectivity spectra for electric vector  $\vec{E}$  parallel to  $\vec{a}$ ,  $\vec{b}$ , or  $\vec{c}$  of SnS and SnSe, respectively. The number of phonons observed for each polarization is consis-

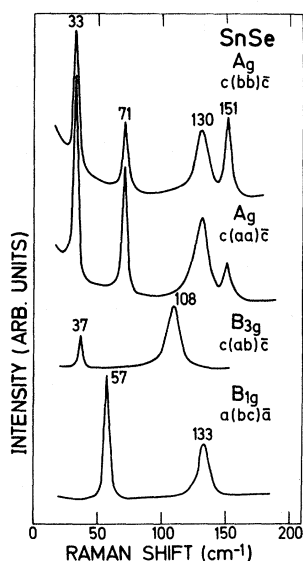


FIG. 2. Room-temperature Raman spectra of SnSe. The comments in the caption of Fig. 1 apply here also.

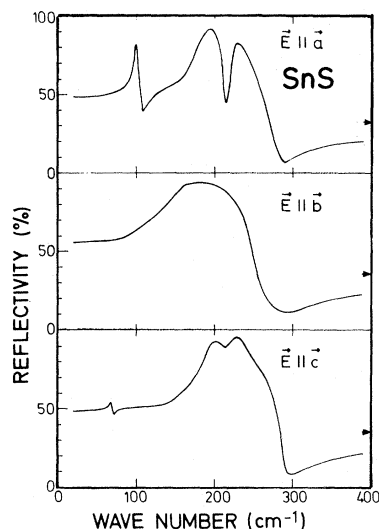


FIG. 3. Room-temperature reflectivity spectra of SnS for three principal polarizations. The arrows at the right-hand side indicate the value of reflectivity measured at  $4000 \text{ cm}^{-1}$ .

tent with group-theoretical predictions (Table II). Though the spectra were measured up to  $4000 \text{ cm}^{-1}$ , the structureless region is not shown in the figures. The reflectivity obtained at  $4000 \text{ cm}^{-1}$  is indicated by an arrow at the right-hand edges of these figures. Assuming a constant value of reflectivity below  $20 \text{ cm}^{-1}$  and above  $4000 \text{ cm}^{-1}$ , the optical constants were obtained by Kramers-Kronig analysis followed by inversion of Fresnel's formula for reflection. The real and imaginary parts  $\epsilon'$  and  $\epsilon''$  of the complex dielectric function

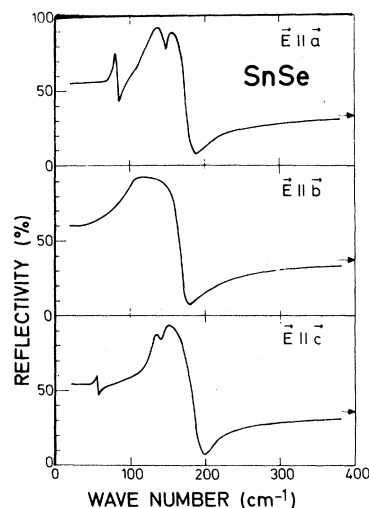


FIG. 4. Room-temperature reflectivity spectra of SnSe. The comments in the caption of Fig. 3 apply here also.

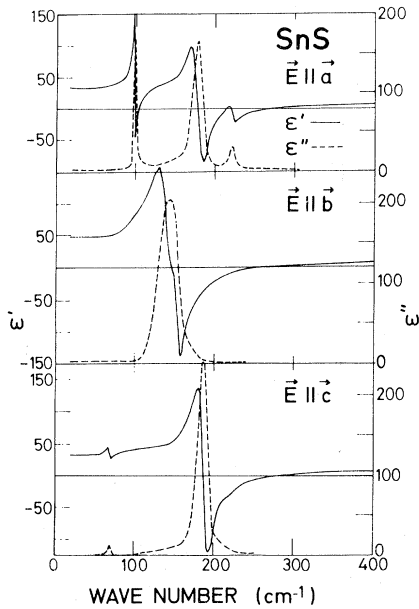


FIG. 5. Real and imaginary parts  $\epsilon'$  and  $\epsilon''$  of the complex dielectric function of SnS obtained from the Kramers-Kronig analysis of the infrared reflectivity data.

$\hat{\epsilon}$  thus obtained are shown in Figs. 5 and 6 for SnS and SnSe, respectively. The maxima in the  $\epsilon''$  spectra occur at the TO frequencies and the above resonance zero crossings of the  $\epsilon'$  spectra occur at the LO phonon frequencies if the phonons are

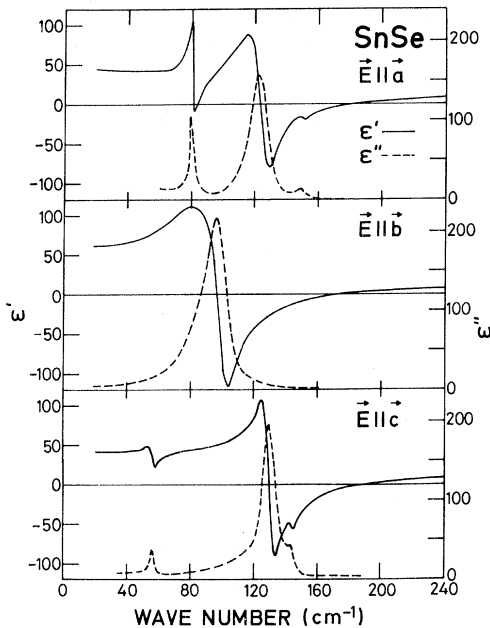


FIG. 6.  $\epsilon'$  and  $\epsilon''$  of SnSe. The comments in the caption of Fig. 5 apply here also.

TABLE III. Phonon frequencies (in  $\text{cm}^{-1}$ ) and dielectric constants of SnS as determined from a Kramers-Kronig analysis of the infrared reflectivity from 20 to  $4000 \text{ cm}^{-1}$ .

	$\vec{E} \parallel \vec{a}$	$\vec{E} \parallel \vec{b}$	$\vec{E} \parallel \vec{c}$
TO <sub>1</sub>	99 ± 5	•••	69 ± 5
LO <sub>1</sub>	107 ± 5	•••	71 ± 5
TO <sub>2</sub>	178 ± 5	•••	188 ± 5
LO <sub>2</sub>	215 ± 5	•••	193 ± 5
TO <sub>3</sub>	222 ± 5	145 ± 5	220 ± 10
LO <sub>3</sub>	277 ± 5	265 ± 5	289 ± 10
$\epsilon_0$	32 ± 4	48 ± 5	32 ± 4
$\epsilon_\infty$	14 ± 2	16 ± 2	16 ± 2

not damped. However, it becomes difficult to evaluate the LO frequencies for phonons which are heavily damped. In these cases the longitudinal modes can be assigned to the peaks of the dielectric-loss function ( $-\text{Im}\hat{\epsilon}^{-1}$ ). The values of LO and TO frequencies and the static and high-frequency dielectric constants,  $\epsilon_0$  and  $\epsilon_\infty$ , are shown in Tables III and IV for SnS and SnSe, respectively.

#### IV. DISCUSSION

We shall briefly return to Table II in order to discuss the implications of our results. The column labeled "Layer symmetry" assumes two adjacent but decoupled layers with symmetry  $C_{2v}$ . The degeneracies of a given mode per layer are also shown in this column. As the interlayer coupling is turned on, the phonons of symmetries corresponding to the point group  $C_{2v}$  split into even ( $g$ ) and odd ( $u$ ) modes according to the symmetry of the point group  $D_{2h}$ . The splitting of the infrared (odd) and Raman-active (even) doublets is a measure of the strength of the interlayer interaction. The translation modes of the "layer" ( $A_1, B_1, B_2$ ) split into translation modes ( $B_{1u}, B_{2u}, B_{3u}$ ) and low-lying optic modes in the crystal. Of these, two

TABLE IV. Phonon frequencies (in  $\text{cm}^{-1}$ ) and dielectric constants of SnSe as determined from a Kramers-Kronig analysis of the infrared reflectivity from 20 to  $4000 \text{ cm}^{-1}$ .

	$\vec{E} \parallel \vec{a}$	$\vec{E} \parallel \vec{b}$	$\vec{E} \parallel \vec{c}$
TO <sub>1</sub>	80 ± 5	•••	56 ± 5
LO <sub>1</sub>	85 ± 5	•••	57 ± 5
TO <sub>2</sub>	123 ± 5	•••	130 ± 5
LO <sub>2</sub>	149 ± 5	•••	141 ± 5
TO <sub>3</sub>	150 ± 5	96 ± 5	142 ± 10
LO <sub>3</sub>	180 ± 5	172 ± 5	191 ± 10
$\epsilon_0$	45 ± 5	62 ± 6	42 ± 5
$\epsilon_\infty$	13 ± 2	17 ± 2	16 ± 2

TABLE V. Comparison of Raman- and infrared-active frequencies (in  $\text{cm}^{-1}$ ) of SnS which are split according to Table II.

$A_g$	$B_{1u}$	$B_{3g}$	$B_{2u}$	$B_{2g}$	$B_{3u}$
$218 \pm 2$	$222 \pm 5$	$164 \pm 2$	$145 \pm 5$	$290 \pm 4$	$220 \pm 10$
$192 \pm 2$	$178 \pm 5$	...	...	$160 (?)$	$188 \pm 5$
$95 \pm 2$	$99 \pm 5$	...	...	$85 \pm 2$	$69 \pm 5$

are rigid shear modes of a layer with respect to its neighbors in the  $\vec{a}$  and  $\vec{b}$  directions ( $A_g, B_{3g}$ ) and the other is a compressive mode of the layers along the  $c$  axis ( $B_{2g}$ ). The layers should also have as their high-frequency modes NaCl-type vibrations in which the Sn atoms vibrate against the S or Se atoms ( $A_1, B_1, B_2$ ). The remaining two  $B_1$  and the two  $A_2$  modes are due to intralayer compression and shear along the  $\vec{a}$  and  $\vec{b}$  axes, respectively. The two intermediate  $A_1$  modes can be described as "breathing" and "waving" modes of the layer.

A comparison of Raman- and infrared-active frequencies split according to the predictions of Table II is presented in Tables V and VI for SnS and SnSe, respectively. The  $B_{2g}$  modes of SnSe were not observed. Hence a comparison with those of  $B_{3u}$  is not possible. Most of the Davydov pairs with the exception of the  $B_{2g}$  and  $B_{3u}$  pairs of SnS are nearly degenerate. The  $290\text{-cm}^{-1}$  line observed in the  $B_{2g}$  configuration is the highest-frequency line in the entire spectrum of SnS. It is not clear whether this line is a second order mode or actually a  $B_{2g}$  mode. In the latter case the Davydov splitting is much too large to be considered as a perturbation. The weak structure near  $160\text{ cm}^{-1}$  was observed in some measurements only. The presence of this line should be treated with caution.

The ratios of intralayer to interlayer force constants can be estimated by assuming a chain of double layers, each characterized by a mass  $M$  and an intralayer force constant  $k$ , coupled along

TABLE VI. Comparison of Raman- and infrared-active frequencies (in  $\text{cm}^{-1}$ ) of SnSe which are split according to Table II.

$A_g$	$B_{1u}$	$B_{3g}$	$B_{2u}$
$151 \pm 2$	$150 \pm 5$	$108 \pm 2$	$96 \pm 5$
$130 \pm 2$	$123 \pm 5$	...	...
$71 \pm 2$	$80 \pm 5$	...	...

the  $c$  axis via an interlayer force constant  $q$ . The frequencies of the rigid-layer mode  $\Omega$  and the infrared-active mode  $\omega$  of the Davydov doublet are  $(2q/M)^{1/2}$  and  $(2k/M)^{1/2}$ , respectively. The Raman mode will be split from the infrared mode by  $(\omega q/2k)$  for  $q \ll k$ . The ratio  $(k/q = \omega^2/\Omega^2)$ , obtained for the electric vector  $\vec{E}$  along  $\vec{a}$ ,  $\vec{b}$ , and  $\vec{c}$  axes, are shown in Table VII for SnS and SnSe. The ratio  $k/q$  for the intralayer vibration along  $\vec{a}$  is nearly the same for all four compounds and is consistently larger than that for the  $\vec{b}$  and  $\vec{c}$  directions. The ratio  $k/q$  deduced from the Davydov splittings shows a large range of values, especially for cases in which the splitting is small and is comparable to the errors in the measurement of Raman- or infrared-active modes. Hence, we believe the estimates using the rigid-layer frequencies are more reliable.

A comparison of the Raman spectra of GeS, GeSe, SnS, and SnSe shows a general similarity for the corresponding modes in different materials with the marked exception of the  $B_{2g}$  modes. There is no discernible pattern in the frequencies of the  $B_{2g}$  modes of GeS, GeSe, and SnS. These modes were too weak to be observed for SnSe.

Figure 7 shows a plot of the infrared- and Raman-active frequencies of SnSe against the corresponding ones of SnS. Also shown in the same figure is a plot of the phonon frequencies of GeSe versus the corresponding ones of GeS. The solid lines passing through the data for low and high frequencies are obtained using a linear fit to the rigid-layer modes and the NaCl-type high-frequen-

TABLE VII. Ratios of intralayer-to-interlayer force constants,  $k/q = (\omega/\Omega)^2$ , of GeS, GeSe, SnS, and SnSe (see text).

	$\vec{E} \parallel \vec{a}$			$\vec{E} \parallel \vec{b}$			$\vec{E} \parallel \vec{c}$		
	$\Omega$	$\omega$	$(k/q)$	$\Omega$	$\omega$	$(k/q)$	$\Omega$	$\omega$	$(k/q)$
GeS <sup>a</sup>	$48 \pm 2$	$258 \pm 5$	$29 \pm 4$	$55 \pm 2$	$201 \pm 5$	$13 \pm 2$	$76 \pm 2$	$280 \pm 5$	$14 \pm 2$
GeSe <sup>b</sup>	$39 \pm 2$	$186 \pm 5$	$23 \pm 4$	$39 \pm 2$	$150 \pm 5$	$15 \pm 2$	$49 \pm 2$	$298 \pm 5$	$16 \pm 2$
SnS	$40 \pm 2$	$222 \pm 5$	$31 \pm 5$	$49 \pm 2$	$145 \pm 5$	$9 \pm 1$	$70 \pm 2$	$220 \pm 10$	$10 \pm 2$
SnSe	$33 \pm 2$	$150 \pm 5$	$21 \pm 4$	$37 \pm 2$	$96 \pm 5$	$7 \pm 1$	...	$142 \pm 10$	...

<sup>a</sup> See Ref. 4.<sup>b</sup> See Ref. 11.

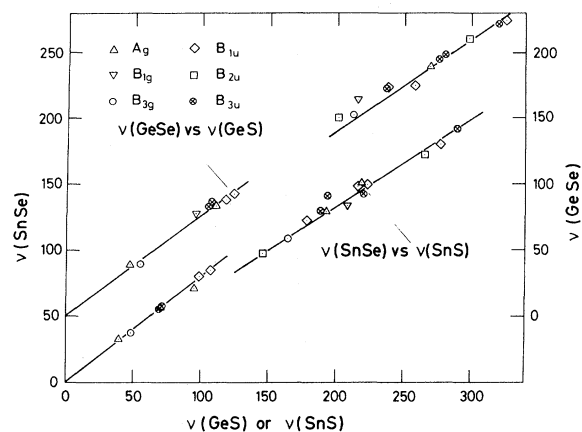


FIG. 7. Phonon frequencies (in  $\text{cm}^{-1}$ ) of Raman- and infrared-active modes of SnSe are plotted against the corresponding ones of SnS. A similar plot of the phonon frequencies (in  $\text{cm}^{-1}$ ) of GeSe vs GeS is also shown (see Refs. 4 and 11). The solid lines are the result of a linear least-squares fit through the data points. Note the origin for the data of  $\nu(\text{GeSe})$  vs  $\nu(\text{GeS})$  is shifted vertically for clarity.

cy modes, respectively, by the method of least squares.<sup>25</sup> The slopes of the lines fitting the data for low frequencies are higher than those for the high-frequency modes. This is not surprising in view of the fact that the low-frequency modes would be determined by the sum of the masses of the constituent atoms whereas the high-frequency modes would be determined by the reduced mass.

It has been shown<sup>26,27</sup> that in the sequence of a family of elements (for example, Si, Ge, and  $\alpha$ -Sn), the phonon frequency  $\nu$  varies as  $r^{-3/2}M^{-1/2}$ , where  $r$  and  $M$  are the lattice constant and atomic mass, respectively. However, under hydrostatic compression  $\nu$  varies as  $r^{-3}M^{-1/2}$ , the difference being attributed to hard core effects.<sup>27</sup> In the sequence of compounds  $\text{Mg}_2\text{X}$ , with  $\text{X} = \text{Si}, \text{Ge},$  or  $\text{Sn}$ ,  $\nu$  is shown<sup>28</sup> to vary as  $r^{-n}M^{-1/2}$ , where  $n$  is a weighted average of  $\frac{3}{2}$  and 3. Using a similar approach one may argue that the ratio of the phonon frequencies of corresponding modes of SnS and SnSe,  $\nu(\text{SnS})/\nu(\text{SnSe})$ , should vary as  $[\nu(\text{SnS})/\nu(\text{SnSe})]^{-n}(M_{\text{SnS}}/M_{\text{SnSe}})^{-1/2}$ . Here  $\nu(\text{SnS})/\nu(\text{SnSe})$  is an average of the ratios of the lattice constants  $a, b,$  and  $c$  of SnS and SnSe. For  $M$ , the sum of the atomic masses of constituent atoms are taken for rigid-layer modes and the reduced masses for high-frequency modes. A similar analysis can be performed for GeS vs GeSe. The average value of  $n$  thus deduced for  $\nu(\text{GeSe})$  vs  $\nu(\text{GeS})$  and  $\nu(\text{SnSe})$  vs  $\nu(\text{SnS})$  for both low- and high-frequency regimes is  $2.2 \pm 0.4$ . Following the argument of Ref. 28,  $n$  would be the average of  $\frac{3}{2}$  and 3, i.e., 2.3, in good agreement with the value obtained from the ex-

perimental data.

A plot of  $\nu(\text{GeS})$  vs  $\nu(\text{SnS})$  or  $\nu(\text{GeSe})$  vs  $\nu(\text{SnSe})$  exhibits a larger scatter from a linear behavior than that of Fig. 7. This scatter is perhaps due to the fact that for the GeS-SnS and GeSe-SnSe pairs, the ratio of lattice constants depends strongly on the direction. For instance, the lattice constants along  $\vec{b}$  of GeS and SnS differ by  $\sim 9\%$  while along  $\vec{a}$  the difference is only  $\sim 1\%$ . Such drastic differences are not found for the pair of compounds with a common cation. The average value of  $n$  deduced from  $\nu(\text{GeS})$  vs  $\nu(\text{SnS})$  and  $\nu(\text{GeSe})$  vs  $\nu(\text{SnSe})$  for the NaCl type and the rigid-layer modes is  $\sim 2.3$  and  $\sim 0$ , respectively. The low value of  $n$  for the latter is perhaps due to the above mentioned problems.

In Fig. 8 we present a comparison of the infrared reflectivity spectra of GeS, GeSe, SnS, and SnSe for  $\vec{E}$  parallel to  $\vec{a}, \vec{b},$  or  $\vec{c}$ . As the constituent atoms get heavier the spectra shift towards lower frequencies. Three phonons are expected for  $\vec{E} \parallel \vec{a}$ , one for  $\vec{E} \parallel \vec{b}$  and three for  $\vec{E} \parallel \vec{c}$ . With the exception of  $\vec{E} \parallel \vec{a}$  for GeS the data are consistent with group-theoretical predictions (Table II). The spectra for all three principal directions contain a dominant reststrahlen band due to the NaCl-type vibration in which the Ge or Sn ion vibrates against the S or Se ion. However, the oscillator strengths of the low- and intermediate-frequency phonons vary considerably from material to material, and also for different polarizations. For example, the phonon in the vicinity of the NaCl-type band is not observed in GeS for  $\vec{E} \parallel \vec{a}$  while it is strong for

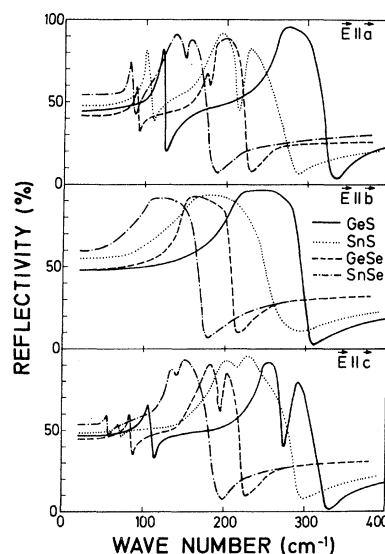


FIG. 8. Comparison of the room-temperature reflectivity spectra of GeS, SnS, GeSe, and SnSe for  $\vec{E}$  parallel to  $\vec{a}, \vec{b},$  and  $\vec{c}$  (see Refs. 4 and 11).

$\vec{E} \parallel \vec{c}$ . On the other hand the reverse is true for SnS. The low-frequency phonon for  $\vec{E} \parallel \vec{a}$  and  $\vec{E} \parallel \vec{c}$  is weaker in GeSe, SnS, and SnSe than in GeS. A complete theoretical analysis is required to understand this complex behavior.

#### V. CONCLUDING REMARKS

The marked similarity in the spectra of zone-center optical phonons, with the exception of the  $B_{2g}$  modes, for GeS, GeSe, SnS, and SnSe discussed in this paper underlines the close relationships in the vibrational properties of these materials. It is not clear why the  $B_{2g}$  modes are much weaker than the other Raman-active modes. An explanation should be sought in a group-theoretical selection rule which forbids the interaction of the  $B_{2g}$  phonons with the electronic gaps mainly responsible for the strong Raman scatter-

ing. Not enough is known about the electronic structure of these compounds to pursue this line of reasoning.

A rough estimate of the various ratios of intra-layer-to-interlayer force constants emphasizes the layerlike character. However, the electron-energy-loss spectra<sup>8,21</sup> do not indicate any anisotropy in the  $\epsilon''$  spectrum above 3 eV: nearly three-dimensional behavior is observed in the electronic properties at high energies.

#### ACKNOWLEDGMENTS

We gratefully acknowledge stimulating discussions with A. Frey and J. D. Wiley. We thank E. Schönherr and W. Stetter for the single crystals, G. Fröhlich and A. Kaiser for orienting and polishing the samples, and A. Breitschwerdt and W. König for technical assistance.

<sup>1</sup>A. Okazaki, J. Phys. Soc. Jpn. **13**, 1151 (1958).

<sup>2</sup>W. Hofmann, Z. Kristallogr. **91**, 161 (1935).

<sup>3</sup>A. Okazaki and I. Uada, J. Phys. Soc. Jpn. **11**, 470 (1956).

<sup>4</sup>J. D. Wiley, W. J. Buckel, and R. L. Schmidt, Phys. Rev. B **13**, 2479 (1976), see Refs. 1–12 in the above for previous work on GeS.

<sup>5</sup>I. Gregora and W. Stetter, Phys. Status Solidi B **71**, K187 (1975).

<sup>6</sup>J. D. Wiley, A. Breitschwerdt, and E. Schönherr, Solid State Commun. **17**, 355 (1975).

<sup>7</sup>J. D. Wiley, W. J. Buckel, W. Braun, G. W. Fehrenbach, F. J. Himpfel, and E. E. Koch, Phys. Rev. B **14**, 697 (1976).

<sup>8</sup>H. Venghaus and U. Büchner, Phys. Status Solidi B **72**, 603 (1975).

<sup>9</sup>S. Asanabe and A. Okazaki, J. Phys. Soc. Jpn. **15**, 989 (1960).

<sup>10</sup>J. M. Chamberlain, S. S. Sirbegović, and P. M. Nikolić, J. Phys. C **7**, L150 (1974).

<sup>11</sup>H. R. Chandrasekhar and U. Zwick, Solid State Commun. **18**, 1509 (1976).

<sup>12</sup>D. I. Siapakas, D. S. Kyriakos, and N. A. Economou, Solid State Commun. **19**, 765 (1976).

<sup>13</sup>S. V. Vlachos, A. P. Lambros, and N. A. Economou, Solid State Commun. **19**, 759 (1976).

<sup>14</sup>W. Albers, C. Haas, H. Ober, G. R. Schodder, and J. D. Wasscher, J. Phys. Chem. Solids, **23**, 215 (1962).

<sup>15</sup>W. Albers, C. Haas, H. J. Vink, and J. D. Wasscher, J. Appl. Phys. **32**, 2220 (1961).

<sup>16</sup>A. P. Lambros, D. Geralaes, and N. A. Economou, J. Phys. Chem. Solids **35**, 537 (1974).

<sup>17</sup>P. M. Nikolic, S. S. Vujatovic, O. H. Hughes, C. J. Doran, and J. M. Chamberlain, in *Proceedings of the XIII International Conference on Physics of Semicon-*

*ductors, Stuttgart, July 15–19, 1974*, edited by M. H. Pilkuhn (Teubner, Stuttgart, 1974), p. 331.

<sup>18</sup>C. Haas and M. M. G. Corbey, J. Phys. Chem. Solids, **20**, 197 (1961).

<sup>19</sup>S. Asanabe, J. Phys. Soc. Jpn. **14**, 281 (1959).

<sup>20</sup>T. Arai, H. M. Onomichi, K. Kubo, in *Proceedings of the International Conference on the Physics and Chemistry of Semiconductor Heterojunctions and Layer Structures*, edited by G. Sziget (Akademical Kiado, Budapest, 1971), Vol. IV, p. 51.

<sup>21</sup>R. Eymard and A. Otto (unpublished).

<sup>22</sup>A. Frey, W. Kress, and R. Zeyher (unpublished).

<sup>23</sup>E. A. Wood, Bell Syst. Tech. J. **43**, 541 (1964). In this notation the relevant diperiodic group is DG32.

<sup>24</sup>It should be noted that the notation used for the group-theoretical representations is not the same in Refs. 5 and 12 which differs from Refs. 4 and 11. Our notation is consistent with Refs. 4 and 11. We denote  $x=c$ ,  $y=b$ ,  $z=a$ . The notation for character tables for  $D_{2h}$  and  $C_{2v}$  and the correlation tables are from E. B. Wilson, J. C. Decius, and P. C. Cross, *Molecular Vibrations* (McGraw-Hill, New York, 1955), pp. 325, 327, and 335.

<sup>25</sup>It should be noted that a similar scaling relation was observed between the frequencies of  $As_2S_3$  and  $As_2Se_3$  crystals which are also layerlike, despite the complexity of their crystal structure. A close similarity between the corresponding eigenvectors was suggested as the reason for such a simple relation. R. Zallen and M. Slade, Phys. Rev. B **9**, 1627 (1974).

<sup>26</sup>R. M. Martin, Phys. Rev. B **1**, 4005 (1970).

<sup>27</sup>C. J. Buchenauer, M. Cardona, and F. H. Pollak, Phys. Rev. B **3**, 1243 (1971).

<sup>28</sup>C. J. Buchenauer and M. Cardona, Phys. Rev. B **3**, 2504 (1971).